Neurostructural Heterogeneity in Youth With Internalizing Symptoms

SUPPLEMENTARY INFORMATION

Table of Contents

Participants

A total of 1,601 participants 8-23 years of age received multi-modal neuroimaging, clinical phenotyping, and cognitive assessment as part of the Philadelphia Neurodevelopmental Cohort (PNC), a large community-based sample of youth (1, 2). From the pool of 1,601 participants, 154 were ineligible for the current study due to: 1) medical disorders that could impact brain functioning (n=81), 2) medication use that could affect central nervous system functioning (n=64), 3) incidentally discovered structural brain abnormalities (3) (n=20), or 4) failing to meet structural image quality assurance protocols (4) (n=51); several subjects were ineligible for multiple criteria. Additionally, two participants were missing clinical diagnostic data, 17 were missing data on maternal level of education, and three were missing cognitive data. These participants were excluded from all analyses. Finally, a subsample of the data (n=282) with information about gestational age at birth was used to examine group differences in birth history. Gestational age, which was defined as the number of weeks of gestation at the time of birth, was determined from a retrospective review of two electronic medical records systems (5).

Clinical assessment

As described in detail in our previous work (1, 2, 6), assessment of lifetime psychopathology was conducted using GOASSESS, a structured screening interview administered to probands (age 11-21) and collateral informants of probands (age 8-17), based on a modified version of the *Kiddie-Schedule for Affective Disorders and Schizophrenia* (7) and *Diagnostic and Statistical Manual of Mental Disorders, 4th edition, Text Revision criteria* (8). The GOASSESS interview assesses lifetime occurrence of mood (major depressive episode, mania), anxiety (agoraphobia, generalized anxiety, panic, specific phobia, social phobia, separation anxiety, posttraumatic stress), behavioral problems (oppositional defiant, attention deficit/hyperactivity, conduct), psychosis, eating disorder (anorexia, bulimia), and suicidal symptoms. Of note, due to comorbidity, participants may be represented in more than one diagnostic category. The GOASSESS interview was administered by trained assessors who underwent a common training protocol (developed and implemented by Dr. Calkins) that included didactic sessions, assigned readings, and supervised pair-wise practice. Assessors were certified for independent assessments following observation by a certified clinical observer who rated the proficiency of the assessor on a 60-item checklist of interview procedures. The median interval of time between clinical assessment and neuroimaging was 2 months.

Clinical and cognitive factor analyses

To provide a dimensional summary of the psychopathology data, we applied an exploratory factor analysis to 112 item-level symptom questions from the GOASSESS interview, which has been described in detail elsewhere (9). This exploratory factor analysis yielded four correlated dimensions of psychopathology including factors for anxious-misery, psychosis, behavioral (externalizing), and fear. We then used a confirmatory bifactor analysis (10, 11) implemented in Mplus (12) to orthogonally model the four factors plus overall psychopathology, which represents the symptoms common across all psychiatric disorders. These orthogonal factors from the bifactor analysis were used in the present study. For the distribution of the individual GOASSESS interview items within the factors, see our previous publication (9).

Cognition was assessed using the University of Pennsylvania Computerized Neurocognitive Battery (CNB), which has been described previously (13). Briefly, 14 cognitive tests evaluating aspects of cognition, including executive control, episodic memory, complex reasoning, social cognition, and sensorimotor speed, were administered in a fixed order. Except for two sensorimotor tests that only measure speed, each test provides measures of both accuracy and speed. We used a measure of overall accuracy, which is the general factor derived from a previously reported bifactor analysis and represents the total accuracy across the 12 accuracy scores (13). To better understand differences in overall accuracy, we also used three factor scores for performance accuracy derived in a previously reported (13) exploratory factor analysis with oblique rotation: 1) executive function and complex reasoning, 2) social cognition, and 3) episodic memory. Reading skills were measured with the *Wide Range Achievement Test, 4th Edition* (WRAT-4) reading subscale with scores reported as T-scores (14).

Image acquisition and processing

Volume and cortical thickness imaging

Imaging data were acquired on a Siemens TIM Trio 3 Tesla scanner (Erlangen, Germany) with a 32-channel head coil. Structural brain imaging was completed using a magnetization-prepared, rapid acquisition gradient-echo (MPRAGE) T1-weighted image with the following parameters: TR = 1810 ms; TE = 3.51 ms; FoV = 180 x 240 mm; matrix 192 x 256; 160 slices; slice thickness/gap 1/0 mm; TI 1100 ms; flip angle 9 degrees; effective voxel resolution of 0.93 x 0.93 x 1.00 mm; total acquisition time 3:28 minutes. Both volume and cortical thickness image processing utilized Advanced Normalization Tools (ANTs) (15). This pipeline includes N4 bias field correction, brain extraction, Atropos probabilistic tissue segmentation (15), and direct estimation of cortical

thickness in volumetric space (16). Large-scale evaluation studies have shown that this highly accurate procedure for estimating cortical thickness is more sensitive to individual differences over the lifespan than comparable techniques (17). Structural images were registered to a custom template using the top-performing SyN diffeomorphic registration method (18). In order to parcellate the brain into anatomically-defined regions, we used an advanced multi-atlas labelling approach. Specifically, 24 young adult T1 images from the OASIS data set that were manually labeled by Neuromorphometrics, Inc. (http://Neuromorphometrics.com/) were registered to each subject's T1 image using the top-performing SyN diffeomorphic registration (18, 19). These label sets were synthesized into a final subject-level parcellation using the top-performing joint label fusion (JLF) segmentation procedure (20).

Resting-state fMRI

Approximately 6 minutes of task-free functional data were acquired for each subject using a blood oxygen level-dependent (BOLD-weighted) sequence (TR = 3000 ms; TE =32 ms; FoV = 192 × 192 mm; resolution 3 mm isotropic; 124 spatial volumes). Subjects were instructed to stay awake, keep their eyes open, fixate on the displayed crosshair, and remain still. Task-free functional images were processed using previously described methods (21). Briefly, preprocessing included 1) correction for distortions induced by magnetic field inhomogeneities using FSL's FUGUE utility, 2) removal of the 4 initial volumes of each acquisition, 3) realignment of all volumes to a selected reference volume using MCFLIRT (22), 4) demeaning and removal of any linear or quadratic trends, 5) co-registration of functional data to the high-resolution structural image using boundary-based registration (23), and 6) temporal filtering using a first-order Butterworth filter with a passband between 0.01 and 0.08 Hz. These preliminary processing stages were then followed by the confound regression procedures, as described previously (21). Briefly, motion artifact in the resting state data was modelled as a linear combination of 36 timeseries: 6 realignment parameters estimated during preprocessing (x-, y-, and z-translations, roll, pitch, yaw), the mean timeseries in deep white matter, the mean timeseries in deep cerebrospinal fluid, the mean signal across the entire brain (global signal), the first temporal derivative of the above timeseries, and quadratic expansions of the above timeseries. In order to prevent frequency-dependent mismatch during confound regression (24), all regressors were band-pass filtered to retain the same frequency range as the data.

Functional connectivity among brain regions is primarily attributable to correlations between low-frequency fluctuations in regional activation patterns. The voxel-wise amplitude of low-frequency fluctuations (ALFF) was computed as the sum over frequency bins in the low-frequency (0.01-0.08 Hertz) band of the voxel-

wise power spectrum, computed using a Fourier transform of the time-domain of the voxel-wise signal (25). ALFF was calculated on data smoothed in SUSAN (26) using a Gaussian-weighted kernel with 6mm FWHM.

Diffusion tensor imaging

DTI scans were acquired using a twice-refocused spin-echo (TRSE) single-shot echo-planar imaging (EPI) sequence (TR = 8100 ms; TE = 82 ms; FoV = 240 x 240 mm^2; Matrix = RL:128/AP:128/Slices:70, in-plane resolution (x and y) 1.875 mm^2; slice thickness = 2mm, gap = 0; flip angle = 90º/180º/180º, volumes = 71, GRAPPA factor = 3, bandwidth = 2170 Hz/pixel, PE direction = AP). This sequence used a four-lobed diffusion encoding gradient scheme combined with a 90-180-180 spin-echo sequence designed to minimize eddy-current artifacts. DTI data were acquired in two consecutive series consisting of 32 diffusion encoding gradient schemes. The complete sequence consisted of 64 diffusion weighted directions with b=1000 s/mm^2 and 7 interspersed scans where b=0 s/mm^2. The duration of DTI scans was approximately 11 minutes. The imaging volume was prescribed in axial orientation covering the entire cerebrum with the topmost slice just superior to the apex of the brain (2). In addition to the DTI scan, a map of the main magnetic field (i.e., B0) was derived from a double-echo, gradient-recalled echo (GRE) sequence, allowing us to estimate field distortions in each dataset.

Two consecutive 32-direction acquisitions were merged into a single 64-direction timeseries. The skull was removed for each subject by registering a binary mask of a standard fractional anisotropy (FA) map (FMRIB58 FA) to each subject's DTI image using a rigid body transformation. Eddy currents and subject motion were estimated and corrected using FSL's eddy tool (27). Diffusion gradient vectors were then rotated to adjust for subject motion estimated by eddy. After the field map was estimated, distortion correction was applied to DTI data using FSL's FUGUE (28). Lastly, the diffusion tensor and fractional anisotropy were estimated at each voxel using the DTIFIT procedure in FSL's Diffusion Toolbox (FDT) (28).

Registration from native space to a template space was completed using DTI-TK (29, 30). First, the DTI outputs (e.g. FA maps) of DTIFIT were converted to DTI-TK format. Next, a template was generated from the tensor volumes using 14 representative diffusion data sets that were considered "excellent" from the PNC sample; the details of this procedure are published (31). Ultimately, one high-resolution refined template was created and used for registration of the remaining diffusion datasets. All DTI maps were then registered to the high-resolution study-specific template using DTI-TK. Standard regions of interest (ICBM-JHU White Matter Tracts) were registered from MNI152 space to the study-specific template using ANTs registration (18). Finally, mean FA was calculated over each white matter tract.

Image quality assurance

Volume and cortical thickness QA

Three highly trained image analysts independently assessed structural image quality; for full details of this procedure see Rosen et al. (32). Briefly, three raters were trained prior to rating images on an independent training sample of 100 images. All three raters were trained to >85% concordance with faculty consensus ratings. T1 images were rated on a 0-2 Likert scale (0 = unusable images, 1 = usable images with some artifact, and 2 = images with none or almost no artifact). All images with an average rating of 0 were excluded from analyses. We included average quality rating across the three raters as a covariate in the models in order to control for the confounding influence of subtle variation in image quality.

All processed data underwent rigorous quality control as well. Specifically, the volume and thickness of anatomically-defined regions of interest (defined using multi-atlas labeling with joint label fusion) were evaluated for outliers. Outliers were defined as values greater or less than 2.5 standard deviations (SD) from the mean regional value. Participants with an elevated (+2.5 SD) number of regions with outlying volume or cortical thickness values were flagged for manual review. Similarly, a regional laterality index was calculated for both cortical thickness and volume, and participants with an elevated number of regional laterality outliers (+2.5 SD) were flagged for review. Flagged images were then manually viewed by two independent data analysts.

Resting-state fMRI QA

As part of the processing procedure for resting BOLD imaging data, the quality of all acquired images was assessed according to a number of metrics. For each of five quality metrics, a minimal inclusion threshold was established and subjects that failed to meet this threshold were omitted from the final sample. Reasons for exclusion/metrics of quality included: 1) resting data not acquired, 2) number of frames with motion exceeding 0.25 mm (> 20 frames), and 3) mean relative RMS displacement (> 0.2 mm framewise). Voxel-wise coverage was assessed on a regional level. Subject motion was assessed on the basis of outputs from the MCFLIRT motion realignment procedure (22). Two criteria for sample inclusion were obtained from the MCFLIRT output: mean relative displacement and the number of motion spikes. The mean relative displacement indicates the average volume-to-volume motion of the subject according to the root-mean-square metric. The number of motion spikes indicates the number of single frames with relative motion in excess of 0.25 mm according to the root-mean-square metric. For the purposes of resting sample inclusion, hard thresholds were established at 0.2 mm for mean relative RMS displacement and 20 frames for number of spikes. In addition to this exclusion criteria, we used a continuous measure of data quality as a covariate in our statistical analyses. As in our prior work (33, 34), the

primary summary metric of subject motion used for resting-state data was the mean relative RMS (root-mean-squared) displacement calculated during time series realignment using MCFLIRT. This metric was included as a covariate to all resting-state analyses.

Diffusion-weighted imaging QA

Diffusion data quality assurance has been described in detail elsewhere (31). Briefly, this process involved initial visual inspection which was done to ensure data fidelity. Individuals with structural abnormalities were excluded. Additionally, any scans collected without the default scan parameters were excluded. Data passing this initial quality assurance step then underwent manual inspection by a trained analyst who inspected each diffusion series in detail. This manual evaluation determined whether each image would be included.

As prior (31), in addition to this manual evaluation, automated measures of image quality were calculated and used as a covariate in statistical testing. Specifically, the temporal signal-to-noise ratio (SNR) was estimated for each brain voxel using only the 64 b=1000 s/mm2 DTI volumes. The voxel-wise SNR was calculated from the mean and standard deviation of each voxel's intensity, after brain masking and motion correction was measured. Subsequently, the average of all brain voxel temporal SNR was calculated to report a single metric of overall scan SNR, which was used as an additional covariate in diffusion analyses.

Group-level statistical analyses

After parsing subtypes of internalizing youth based on structural data, we sought to 1) define how the subtypes differed on psychopathology and cognition, 2) understand what structural features (thickness, volume) drove the subtypes discovered, and 3) investigate differences between the subtypes in two independent neuroimaging sequences not used in clustering (ALFF from rsfMRI and fractional anisotropy from DTI). Given that brain development is a non-linear process (34–36), we modeled both linear and nonlinear age effects using penalized splines within a generalized additive model (GAM), which assesses a penalty on nonlinearity using restricted maximum likelihood (REML) in order to avoid over-fitting (37, 38). Based on known sex differences in structure (39), we included sex as a covariate in the model. As expected given that internalizing disorders are more common in females, the subtypes showed a greater percentage of females than typically developing youth. Additionally, quality ratings for each imaging modality were added as an additional model covariate to control for the potential confounding effects of image quality (32). Our group variable was modeled as a factor with three

levels: typically developing, Subtype 1 and Subtype 2. We examined group differences in each brain region as follows:

Region = spline(age) + sex + image quality rating + group

Omnibus ANOVAs testing for group differences were corrected for multiple comparisons by controlling the False Discovery Rate (FDR, $Q<0.05$). We then conducted pairwise post-hoc tests (S1 vs. TD, S2 vs. TD, and S1 vs. S2) to determine which groups significantly differed from each other, which were also corrected for multiple comparisons using FDR. Interactions between group and age as well as group and sex were also evaluated. Finally, sensitivity analyses excluding participants who were taking psychotropic medications at the time of imaging (excluded: n=104; included: n=1,037) were conducted to ensure that our results were not driven by medication effects.

Permutation testing of subtypes

Permutation tests are useful tools for assessing statistical significance when the underlying distribution of data is unknown (40). Here we define the null distribution of the subtypes using the healthy control sample, where disease-related variability is not present. For this analysis, half of the healthy controls (n = 426) were randomly assigned to the control group (n=213) and half to the pseudo-patient group (n=213), and these samples were permuted 75 times in HYDRA. We then compared these results to a real-patient group of equal number that included the control samples and real-patient samples (each also equal to n=213). The control and real-patient samples were also permuted 75 times in HYDRA. The clustering stability defined by the adjusted Rand index (ARI) was compared between the subtypes derived from the pseudo-patient (null) and real-patient samples. The ARI for the 2-cluster solution was significantly higher in the real-patient sample compared to that of the null distribution (i.e., pseudo-patient; $p_{fdr} < .001$). The ARIs for the other cluster solutions were not different from the null distribution ($p_{fdr} > 0.05$), except for the 7-cluster solution ($p_{fdr} = 0.014$); however, the stability of 7-cluster solution was substantially lower (ARI of .30). Overall, the permutation testing demonstrated that the 2-cluster solution is significantly more stable than that expected by chance alone.

Supplementary Table S1. Group differences on demographics, cognition, academic achievement, and psychopathology (n=1,141).

			S1-TD				S2-TD				S1-S2			
	F/X^2	p	B	SE	t	p_{fdr}	B	SE	t	p_{fdr}	B	SE	t	p_{fdr}
Age*	3.48	.031	0.67	0.26	2.61	.027	0.42	0.28	1.51	.196	0.26	0.28	0.91	.361
Gender*	10.64	.005	0.43	0.14	3.09	.006	0.34	0.15	2.29	.033	0.09	0.15	0.59	.557
Maternal level of education*	20.56	<.001	-1.01	0.17	-5.99	<.001	-0.12	0.18	-0.67	.503	-0.89	0.18	-4.86	<.001
Trauma exposure*	53.49	<.001	0.84	0.08	10.29	<.001	0.50	0.09	5.61	<.001	0.35	0.09	3.94	<.001
Gestational age at birth†	4.39	.013	-1.54	0.52	-2.95	.011	-0.48	0.58	-0.84	.403	-1.06	0.61	-1.73	.126
Academic achievement^	35.56	<.001	-8.00	1.10	-7.25	<.001	0.61	1.18	0.51	.608	-8.61	1.19	-7.23	<.001
Overall accuracy^	28.47	<.001	-0.29	0.05	-5.68	<.001	0.10	0.05	1.82	.069	-0.38	0.05	-7.07	<.001
Accuracy factors^	F	p_{fdr}	B	SE	t	p_{fdr}	B	SE	t	p_{fdr}	B	SE	t	p_{fdr}
Executive function/complex reasoning	39.26	<.001	-0.37	0.05	-6.97	<.001	0.09	0.06	1.67	.096	-0.47	0.06	-8.12	<.001
Social cognition	6.79	.001	-0.12	0.05	-2.21	.042	0.09	0.06	1.62	.106	-0.21	0.06	-3.65	.001
Episodic memory	7.21	.001	-0.12	0.06	-1.93	.054	0.13	0.06	2.03	.054	-0.25	0.07	-3.79	<.001
Psychopathology factors^	F	p_{fdr}	B	SE	t	p_{fdr}	B	SE	t	p_{fdr}	B	SE	t	p_{fdr}
Anxious-misery	18.38	<.001	0.31	0.07	4.70	<.001	0.39	0.07	5.56	<.001	-0.08	0.07	-1.15	.249
Psychosis	12.17	<.001	0.34	0.07	4.74	<.001	0.25	0.08	3.38	.001	0.08	0.08	1.05	.292
Behavioral	25.46	<.001	0.47	0.07	7.14	<.001	0.23	0.07	3.27	.001	0.24	0.07	3.38	.001
Fear	39.66	<.001	0.58	0.07	8.72	<.001	0.39	0.07	5.59	<.001	0.18	0.07	2.55	.011
Overall psychopathology	250.30	<.001	1.28	0.06	21.02	<.001	1.07	0.06	16.45	<.001	0.21	0.07	3.20	.001

*df=1,138; †df=229; ^df=1,136

Supplementary Table S2. Group differences in volume and cortical thickness (n=1,141, df=1,134).

			S1-TD				S2-TD				S1-S2			
	F	***p***	***B***	***SE***	***t***	p_{fdr}	***B***	***SE***	***t***	p_{fdr}	***B***	***SE***	***t***	p_{fdr}
Intracranial volume	215.56	<.001	-101.02	7.41	-13.64	<.001	59.13	7.85	7.54	<.001	-160.15	7.90	-20.26	<.001
Total brain volume	222.13	<.001	-97.74	7.18	-13.62	<.001	60.21	7.60	7.92	<.001	-157.95	7.66	-20.63	<.001
Total gray matter volume	291.91	<.001	-49.75	3.23	-15.42	<.001	31.86	3.42	9.32	<.001	-81.61	3.44	-23.70	<.001
Average cortical thickness	146.67	<.001	-0.11	0.01	-10.89	<.001	0.07	0.01	6.67	<.001	-0.19	0.01	-16.81	<.001

Supplementary Table S3. Group differences in resting-state ALFF (n=840, df=834).

			S1-TD				S2-TD				S1-S2			
	F	***p***	***B***	***SE***	***t***	p_{fdr}	***B***	***SE***	***t***	p_{fdr}	***B***	***SE***	***t***	p_{fdr}
Right amygdala	12.08	<.001	-0.15	0.04	-4.12	<.001	0.02	0.04	0.46	.649	-0.17	0.04	-4.33	<.001
Left amygdala	4.77	.029	-0.11	0.04	-3.02	.008	-0.03	0.04	-0.82	.413	-0.08	0.04	-2.03	.065
Right hippocampus	6.26	.008	-0.06	0.02	-2.66	.012	0.02	0.02	0.82	.413	-0.08	0.02	-3.33	.003
Right anterior cingulate gyrus	23.87	<.001	-0.25	0.05	-5.52	<.001	0.05	0.05	1.11	.266	-0.30	0.05	-6.29	<.001
Left anterior cingulate gyrus	19.22	<.001	-0.22	0.05	-4.89	<.001	0.05	0.05	1.10	.270	-0.28	0.05	-5.69	<.001
Right anterior insula	5.30	.018	-0.10	0.04	-2.42	.024	0.04	0.04	0.81	.418	-0.14	0.05	-3.07	.007
Right anterior orbital gyrus	12.52	<.001	-0.08	0.05	-1.61	.109	0.17	0.05	3.44	.001	-0.25	0.05	-4.93	<.001
Left anterior orbital gyrus	4.53	.033	-0.03	0.04	-0.76	.446	0.10	0.05	2.23	.039	-0.13	0.05	-2.92	.011
Right angular gyrus	4.73	.029	-0.09	0.05	-1.73	.126	0.08	0.05	1.45	.147	-0.16	0.05	-3.06	.007
Left angular gyrus	5.17	.020	-0.12	0.05	-2.22	.040	0.06	0.06	1.03	.301	-0.17	0.06	-3.11	.006
Right entorhinal area	4.29	.040	-0.10	0.04	-2.68	.023	-0.01	0.04	-0.21	.836	-0.09	0.04	-2.34	.030
Right frontal operculum	8.50	.001	-0.13	0.05	-2.65	.012	0.08	0.05	1.55	.122	-0.21	0.05	-4.04	<.001
Right frontal pole	12.46	<.001	-0.12	0.04	-2.88	.006	0.10	0.04	2.24	.025	-0.22	0.04	-4.96	<.001
Left frontal pole	12.22	<.001	-0.14	0.04	-3.27	.002	0.08	0.05	1.73	.084	-0.22	0.05	-4.83	<.001
Right gyrus rectus	6.49	.007	-0.06	0.03	-1.69	.092	0.07	0.03	2.04	.063	-0.13	0.03	-3.60	.001
Left gyrus rectus	5.98	.010	-0.05	0.04	-1.44	.149	0.08	0.04	2.10	.054	-0.13	0.04	-3.45	.002
Right lateral orbital gyrus	12.75	<.001	-0.03	0.04	-0.64	.522	0.18	0.04	4.12	<.001	-0.20	0.04	-4.69	<.001
Left lateral orbital gyrus	8.23	.002	-0.01	0.05	-0.22	.824	0.16	0.05	3.47	.001	-0.17	0.05	-3.65	.001
Right medial frontal cortex	14.69	<.001	-0.16	0.05	-3.46	.001	0.10	0.05	2.09	.037	-0.26	0.05	-5.32	<.001
Left medial frontal cortex	14.33	<.001	-0.14	0.05	-2.99	.004	0.13	0.05	2.53	.011	-0.27	0.05	-5.33	<.001
Right middle frontal gyrus	16.38	<.001	-0.20	0.06	-3.51	.001	0.14	0.06	2.34	.019	-0.34	0.06	-5.66	<.001
Left middle frontal gyrus	12.23	<.001	-0.18	0.06	-3.07	.003	0.12	0.06	1.98	.048	-0.30	0.06	-4.88	<.001
Right medial orbital gyrus	6.98	.004	-0.06	0.03	-1.98	.063	0.05	0.03	1.86	.063	-0.11	0.03	-3.73	.001
Left medial orbital gyrus	5.49	.015	-0.06	0.03	-2.01	.068	0.04	0.03	1.38	.167	-0.10	0.03	-3.28	.003
Right superior frontal gyrus medial segment	18.03	<.001	-0.26	0.06	-4.58	<.001	0.07	0.06	1.28	.202	-0.33	0.06	-5.62	<.001
Left superior frontal gyrus medial segment	15.85	<.001	-0.25	0.06	-4.34	<.001	0.07	0.06	1.12	.262	-0.32	0.06	-5.24	<.001
Right middle temporal gyrus	4.55	.033	-0.05	0.04	-1.25	.211	0.08	0.04	1.85	.097	-0.13	0.04	-3.01	.008
Right opercular part of the inferior frontal gyrus	12.83	<.001	-0.16	0.06	-2.72	.010	0.15	0.06	2.49	.013	-0.31	0.06	-5.06	<.001
Left opercular part of the inferior frontal gyrus	8.33	.001	-0.14	0.06	-2.26	.037	0.12	0.06	1.95	.052	-0.26	0.06	-4.07	<.001
Right orbital part of the inferior frontal gyrus	5.70	.013	-0.07	0.05	-1.56	.118	0.09	0.05	1.91	.085	-0.16	0.05	-3.38	.002
Left orbital part of the inferior frontal gyrus	4.51	.033	-0.05	0.05	-0.91	.365	0.12	0.05	2.10	.054	-0.16	0.06	-2.94	.010
Right parahippocampal gyrus	4.10	.046	-0.05	0.03	-1.85	.097	0.03	0.03	1.06	.290	-0.08	0.03	-2.81	.015
Right posterior orbital gyrus	6.21	.008	-0.07	0.03	-2.38	.026	0.04	0.03	1.20	.229	-0.11	0.03	-3.42	.002
Right planum polare	6.96	.004	-0.07	0.05	-1.38	.169	0.12	0.05	2.42	.024	-0.19	0.05	-3.70	.001
Right superior frontal gyrus	10.61	<.001	-0.17	0.05	-3.17	.002	0.08	0.06	1.46	.146	-0.25	0.06	-4.46	<.001
Left superior frontal gyrus	7.29	.004	-0.14	0.05	-2.52	.018	0.08	0.06	1.35	.178	-0.22	0.06	-3.73	.001
Left superior parietal lobule	4.15	.045	-0.10	0.05	-1.79	.111	0.07	0.06	1.17	.243	-0.16	0.06	-2.84	.014
Right temporal pole	15.16	<.001	-0.11	0.03	-3.97	<.001	0.05	0.03	1.54	.124	-0.16	0.03	-5.25	<.001
Left temporal pole	9.58	<.001	-0.10	0.03	-3.22	.002	0.03	0.03	1.11	.268	-0.13	0.03	-4.15	<.001
Right triangular part of the inferior frontal gyrus	16.75	<.001	-0.15	0.05	-2.87	.004	0.17	0.06	3.08	.003	-0.32	0.06	-5.79	<.001
Left triangular part of the inferior frontal gyrus	7.50	.003	-0.09	0.06	-1.63	.104	0.14	0.06	2.34	.029	-0.24	0.06	-3.86	<.001

Supplementary Table S4. Group differences in fractional anisotropy of white matter tracts (n=923, df=916).

			S1-TD				S2-TD				S1-S2			
	F	***p***	***B***	***SE***	***t***	p_{fdr}	***B***	***SE***	***t***	p_{fdr}	***B***	***SE***	***t***	p_{fdr}
Left anterior thalamic radiation	7.09	.002	-0.08	0.06	-1.23	.217	0.17	0.07	2.56	.016	-0.25	0.07	-3.72	.001
Right anterior thalamic radiation	5.74	.007	-0.08	0.06	-1.29	.198	0.15	0.07	2.16	.047	-0.23	0.07	-3.37	.002
Right corticospinal tract	3.61	.049	-0.15	0.07	-2.21	.041	0.02	0.07	0.32	.751	-0.18	0.07	-2.40	.041
Left cingulum (hippocampus)	9.88	<.001	-0.24	0.07	-3.44	.001	0.07	0.07	0.89	.373	-0.31	0.07	-4.11	<.001
Right cingulum (hippocampus)	8.66	.001	-0.22	0.07	-3.01	.004	0.09	0.08	1.18	.240	-0.31	0.08	-3.96	<.001
Forceps minor	10.70	<.001	-0.22	0.07	-3.30	.002	0.09	0.07	1.32	.187	-0.31	0.07	-4.42	<.001
Left inferior longitudinal fasciculus	10.66	<.001	-0.29	0.07	-3.96	<.001	0.02	0.08	0.24	.812	-0.31	0.08	-3.97	<.001
Right inferior longitudinal fasciculus	18.82	<.001	-0.34	0.07	-4.60	<.001	0.11	0.08	1.42	.155	-0.46	0.08	-5.76	<.001
Right superior longitudinal fasciculus	7.13	.002	-0.23	0.07	-3.52	.001	-0.03	0.07	-0.46	.644	-0.20	0.07	-2.87	.006
Left uncinate fasciculus	5.96	.006	-0.23	0.07	-3.16	.005	-0.02	0.08	-0.24	.811	-0.21	0.08	-2.73	.010

Supplementary Table S5. Demographics, cognition, academic achievement, and psychopathology sensitivity analyses that exclude those taking psychotropic medications (n=1,037).

			S1-TD				S2-TD				S1-S2			
	F/X^2	*p*	*B*	*SE*	*t*	p_{fdr}	*B*	*SE*	*t*	p_{fdr}	*B*	*SE*	*t*	p_{fdr}
Age*	4.36	.013	0.79	0.27	2.95	.010	0.35	0.29	1.22	.222	0.44	0.30	1.47	.212
Gender*	15.10	<.001	0.55	0.15	3.72	.001	0.40	0.16	2.54	.017	0.15	0.16	0.90	.369
Maternal level of education*	16.90	<.001	-0.95	0.17	-5.45	<.001	-0.10	0.19	-0.53	.595	-0.85	0.19	-4.39	<.001
Academic achievement^	30.27	<.001	-7.80	1.16	-6.74	<.001	0.69	1.24	0.56	.579	-8.49	1.27	-6.66	<.001
Overall accuracy^	22.54	<.001	-0.27	0.05	-5.13	<.001	0.09	0.06	1.65	.098	-0.37	0.06	-6.27	<.001
Accuracy factors^	*F*	p_{fdr}	*B*	*SE*	*t*	p_{fdr}	*B*	*SE*	*t*	p_{fdr}	*B*	*SE*	*t*	p_{fdr}
Executive function/complex reasoning	32.74	<.001	-0.37	0.06	-6.56	<.001	0.08	0.06	1.39	.163	-0.45	0.06	-7.32	<.001
Social cognition	3.55	.029	-0.08	0.06	-1.39	.165	0.09	0.06	1.44	.165	-0.16	0.06	-2.66	.024
Episodic memory	7.88	.001	-0.13	0.06	-1.99	.047	0.15	0.07	2.22	.040	-0.28	0.07	-3.97	<.001
Psychopathology factors^	*F*	p_{fdr}	*B*	*SE*	*t*	p_{fdr}	*B*	*SE*	*t*	p_{fdr}	*B*	*SE*	*t*	p_{fdr}
Anxious-misery	15.58	<.001	0.30	0.07	4.56	<.001	0.35	0.07	4.89	<.001	-0.05	0.07	-0.62	.533
Psychosis	12.08	<.001	0.34	0.07	4.59	<.001	0.28	0.08	3.58	.001	0.06	0.08	0.68	.496
Behavioral	21.46	<.001	0.42	0.07	6.47	<.001	0.13	0.07	1.90	.057	0.29	0.07	4.02	<.001
Fear	41.80	<.001	0.61	0.07	8.88	<.001	0.43	0.07	5.83	<.001	0.18	0.08	2.39	.017
Overall psychopathology	218.31	<.001	1.24	0.06	19.54	<.001	1.04	0.07	15.20	<.001	0.21	0.07	2.95	.003

*df=1,034; ^df=1,032

Supplementary Table S6. Volume and cortical thickness sensitivity analyses that exclude those taking psychotropic medications (n=1,037, df=1,030).

			S1-TD				S2-TD				S1-S2			
	F	***p***	***B***	***SE***	***t***	p_{fdr}	***B***	***SE***	***t***	p_{fdr}	***B***	***SE***	***t***	p_{fdr}
Intracranial volume	183.43	<.001	-97.19	7.73	-12.58	<.001	60.53	8.21	7.38	<.001	-157.72	8.42	-18.74	<.001
Total brain volume	187.92	<.001	-94.46	7.50	-12.60	<.001	60.77	7.96	7.63	<.001	-155.24	8.17	-19.00	<.001
Total gray matter volume	249.86	<.001	-48.23	3.38	-14.27	<.001	32.75	3.59	9.12	<.001	-80.98	3.69	-21.97	<.001
Average cortical thickness	134.91	<.001	-0.12	0.01	-10.79	<.001	0.07	0.01	6.34	<.001	-0.19	0.01	-16.07	<.001

Supplementary Table S7. Resting-state ALFF sensitivity analyses that exclude those taking psychotropic medications (n=763, df=756).

			S1-TD				S2-TD				S1-S2			
	F	***p***	***B***	***SE***	***t***	p_{fdr}	***B***	***SE***	***t***	p_{fdr}	***B***	***SE***	***t***	p_{fdr}
Right amygdala	8.89	.001	-0.14	0.04	-3.67	.001	0.01	0.04	0.23	.818	-0.15	0.04	-3.60	.001
Left amygdala	4.53	.046	-0.12	0.04	-2.95	.010	-0.03	0.04	-0.78	.437	-0.08	0.04	-1.94	.079
Right anterior cingulate gyrus	19.44	<.001	-0.25	0.05	-5.31	<.001	0.03	0.05	0.57	.568	-0.28	0.05	-5.42	<.001
Left anterior cingulate gyrus	14.40	<.001	-0.21	0.05	-4.51	<.001	0.03	0.05	0.61	.545	-0.24	0.05	-4.72	<.001
Right anterior orbital gyrus	11.48	<.001	-0.07	0.05	-1.48	.140	0.18	0.05	3.43	.001	-0.26	0.05	-4.70	<.001
Right frontal operculum	6.54	.009	-0.12	0.05	-2.30	.033	0.08	0.06	1.47	.142	-0.20	0.06	-3.56	.001
Right frontal pole	9.18	.001	-0.11	0.04	-2.54	.017	0.09	0.05	1.95	.051	-0.20	0.05	-4.25	<.001
Left frontal pole	8.48	.002	-0.13	0.05	-2.73	.010	0.07	0.05	1.53	.127	-0.20	0.05	-4.02	<.001
Right gyrus rectus	4.65	.042	-0.04	0.03	-1.22	.223	0.07	0.04	1.97	.075	-0.11	0.04	-3.04	.007
Right lateral orbital gyrus	12.15	<.001	-0.02	0.04	-0.51	.608	0.19	0.05	4.15	<.001	-0.22	0.05	-4.53	<.001
Left lateral orbital gyrus	7.13	.005	0.00	0.05	-0.02	.987	0.17	0.05	3.37	.001	-0.17	0.05	-3.30	.001
Right medial frontal cortex	10.30	<.001	-0.15	0.05	-3.14	.003	0.08	0.05	1.55	.122	-0.23	0.05	-4.39	<.001
Left medial frontal cortex	10.30	<.001	-0.12	0.05	-2.57	.016	0.11	0.05	2.21	.027	-0.24	0.05	-4.52	<.001
Right middle frontal gyrus	10.48	<.001	-0.16	0.06	-2.80	.008	0.12	0.06	1.99	.047	-0.29	0.06	-4.53	<.001
Left middle frontal gyrus	7.86	.003	-0.15	0.06	-2.40	.025	0.11	0.06	1.75	.081	-0.26	0.07	-3.93	<.001
Right medial orbital gyrus	5.43	.024	-0.05	0.03	-1.68	.094	0.06	0.03	1.78	.094	-0.11	0.03	-3.29	.003
Right superior frontal gyrus medial segment	13.14	<.001	-0.24	0.06	-4.11	<.001	0.06	0.06	0.90	.369	-0.30	0.06	-4.68	<.001
Left superior frontal gyrus medial segment	10.79	<.001	-0.23	0.06	-3.82	<.001	0.04	0.06	0.65	.516	-0.27	0.06	-4.17	<.001
Right opercular part of the inferior frontal gyrus	9.27	.001	-0.14	0.06	-2.24	.026	0.15	0.06	2.29	.026	-0.28	0.07	-4.30	<.001
Left opercular part of the inferior frontal gyrus	5.11	.030	-0.10	0.06	-1.65	.099	0.11	0.07	1.71	.099	-0.22	0.07	-3.19	.004
Right orbital part of the inferior frontal gyrus	4.70	.042	-0.06	0.05	-1.17	.244	0.10	0.05	2.01	.067	-0.16	0.05	-3.04	.007
Right posterior orbital gyrus	5.26	.027	-0.07	0.03	-2.28	.034	0.04	0.03	1.06	.290	-0.11	0.04	-3.12	.006
Right superior frontal gyrus	6.60	.009	-0.15	0.06	-2.63	.013	0.06	0.06	1.06	.291	-0.21	0.06	-3.47	.002
Right temporal pole	11.86	<.001	-0.11	0.03	-3.63	<.001	0.04	0.03	1.30	.193	-0.15	0.03	-4.60	<.001
Left temporal pole	7.54	.004	-0.09	0.03	-2.83	.007	0.04	0.03	1.10	.270	-0.13	0.03	-3.70	.001
Right triangular part of the inferior frontal gyrus	11.59	<.001	-0.13	0.06	-2.37	.018	0.16	0.06	2.68	.011	-0.29	0.06	-4.82	<.001
Left triangular part of the inferior frontal gyrus	4.98	.033	-0.06	0.06	-1.00	.316	0.14	0.06	2.23	.039	-0.21	0.07	-3.10	.006

Supplementary Table S8. Fractional anisotropy sensitivity analyses that exclude those taking psychotropic medications (n=836, df=828).

			S1-TD				S2-TD				S1-S2			
	F	***p***	***B***	***SE***	***t***	p_{fdr}	***B***	***SE***	***t***	p_{fdr}	***B***	***SE***	***t***	p_{fdr}
Left anterior thalamic radiation	5.17	.012	-0.07	0.07	-1.03	.301	0.16	0.07	2.25	.037	-0.23	0.07	-3.17	.005
Right anterior thalamic radiation	5.42	.010	-0.09	0.07	-1.30	.192	0.16	0.07	2.11	.052	-0.25	0.07	-3.28	.003
Left cingulum (hippocampus)	8.16	.001	-0.23	0.07	-3.14	.003	0.07	0.08	0.88	.381	-0.30	0.08	-3.74	.001
Right cingulum (hippocampus)	8.59	.001	-0.25	0.08	-3.29	.002	0.07	0.08	0.82	.414	-0.32	0.08	-3.80	<.001
Forceps minor	9.59	<.001	-0.22	0.07	-3.16	.002	0.09	0.07	1.29	.197	-0.31	0.07	-4.18	<.001
Left inferior longitudinal fasciculus	10.25	<.001	-0.31	0.08	-3.97	<.001	0.01	0.08	0.17	.867	-0.32	0.08	-3.82	<.001
Right inferior longitudinal fasciculus	17.84	<.001	-0.36	0.08	-4.61	<.001	0.11	0.08	1.33	.184	-0.47	0.09	-5.55	<.001
Right superior longitudinal fasciculus	7.41	.002	-0.25	0.07	-3.64	.001	-0.04	0.07	-0.51	.607	-0.21	0.08	-2.85	.007
Left uncinate fasciculus	5.77	.008	-0.25	0.08	-3.32	.003	-0.07	0.08	-0.83	.406	-0.18	0.08	-2.24	.038

Supplementary Table S9. Group differences in volume and cortical thickness while controlling for race (n=1,141, df=1,133).

			S1-TD				S2-TD				S1-S2			
	F	***p***	***B***	***SE***	***t***	p_{fdr}	***B***	***SE***	***t***	p_{fdr}	***B***	***SE***	***t***	p_{fdr}
Intracranial volume	149.70	<.001	-77.97	7.26	-10.74	<.001	55.68	7.41	7.52	<.001	-133.65	7.79	-17.16	<.001
Total brain volume	157.35	<.001	-76.89	7.09	-10.85	<.001	57.08	7.23	7.89	<.001	-133.97	7.60	-17.62	<.001
Total gray matter volume	213.98	<.001	-38.84	3.13	-12.42	<.001	30.23	3.19	9.47	<.001	-69.07	3.36	-20.58	<.001
Average cortical thickness	103.07	<.001	-0.09	0.01	-8.67	<.001	0.07	0.01	6.53	<.001	-0.16	0.01	-14.28	<.001

Supplementary Table S10. Group differences in resting-state ALFF while controlling for race (n=840, df=833).

			S1-TD				S2-TD				S1-S2			
	F	***p***	***B***	***SE***	***t***	p_{fdr}	***B***	***SE***	***t***	p_{fdr}	***B***	***SE***	***t***	p_{fdr}
Right amygdala	9.80	<.001	-0.15	0.04	-3.79	<.001	0.02	0.04	0.43	.667	-0.16	0.04	-3.94	<.001
Right caudate	7.77	0.002	-0.10	0.04	-2.29	.033	0.08	0.04	1.91	.057	-0.18	0.05	-3.93	<.001
Left caudate	5.16	0.017	-0.11	0.05	-2.30	.033	0.05	0.05	1.03	.302	-0.15	0.05	-3.12	.006
Right hippocampus	5.34	0.015	-0.06	0.02	-2.49	.019	0.02	0.02	0.81	.418	-0.08	0.03	-3.11	.006
Right pallidum	5.11	0.017	-0.09	0.03	-2.90	.011	<.001	0.03	-0.05	.962	-0.08	0.03	-2.66	.012
Left pallidum	4.54	0.025	-0.08	0.03	-2.49	.019	0.01	0.03	0.44	.661	-0.10	0.03	-2.75	.018
Right putamen	7.93	0.002	-0.14	0.05	-3.12	.003	0.04	0.05	0.89	.371	-0.18	0.05	-3.75	.001
Left putamen	4.79	0.021	-0.11	0.05	-2.51	.019	0.03	0.05	0.56	.578	-0.14	0.05	-2.86	.013
Right anterior cingulate gyrus	19.37	<.001	-0.24	0.05	-5.07	<.001	0.05	0.05	1.08	.281	-0.29	0.05	-5.74	<.001
Left anterior cingulate gyrus	15.29	<.001	-0.21	0.05	-4.44	<.001	0.05	0.05	1.07	.287	-0.26	0.05	-5.14	<.001
Right anterior insula	7.09	0.003	-0.13	0.04	-2.91	.006	0.04	0.04	0.90	.368	-0.17	0.05	-3.56	.001
Right anterior orbital gyrus	10.92	<.001	-0.07	0.05	-1.39	.166	0.17	0.05	3.41	.001	-0.24	0.05	-4.52	<.001
Left anterior orbital gyrus	4.06	0.034	-0.03	0.05	-0.66	.507	0.10	0.05	2.21	.041	-0.13	0.05	-2.70	.021
Right central operculum	5.82	0.010	-0.08	0.06	-1.46	.144	0.12	0.06	2.14	.049	-0.20	0.06	-3.39	.002
Left central operculum	3.61	0.049	-0.10	0.05	-1.91	.084	0.05	0.05	0.88	.380	-0.15	0.06	-2.61	.027
Right entorhinal area	4.81	0.021	-0.11	0.04	-2.86	.013	-0.01	0.04	-0.16	.869	-0.11	0.04	-2.54	.017
Right frontal operculum	6.64	0.005	-0.12	0.05	-2.32	.031	0.08	0.05	1.51	.131	-0.20	0.06	-3.61	.001
Left frontal operculum	4.17	0.032	-0.13	0.05	-2.41	.025	0.02	0.05	0.40	.691	-0.15	0.06	-2.63	.025
Right frontal pole	13.81	<.001	-0.14	0.04	-3.23	.002	0.10	0.04	2.31	.021	-0.24	0.05	-5.23	<.001
Left frontal pole	11.09	<.001	-0.15	0.05	-3.18	.002	0.08	0.05	1.73	.083	-0.23	0.05	-4.63	<.001
Right gyrus rectus	4.56	0.025	-0.04	0.03	-1.21	.227	0.07	0.03	1.97	.073	-0.11	0.04	-2.99	.009
Left gyrus rectus	4.40	0.027	-0.04	0.04	-1.04	.299	0.08	0.04	2.05	.061	-0.12	0.04	-2.91	.011
Right inferior temporal gyrus	4.47	0.026	-0.05	0.03	-1.63	.123	0.05	0.03	1.55	.123	-0.10	0.03	-2.99	.009
Right lateral orbital gyrus	12.15	<.001	-0.03	0.04	-0.63	.527	0.18	0.04	4.12	<.001	-0.21	0.05	-4.48	<.001
Left lateral orbital gyrus	9.24	0.001	-0.03	0.05	-0.65	.514	0.17	0.05	3.53	.001	-0.20	0.05	-3.95	<.001
Right middle cingulate gyrus	7.10	0.003	-0.17	0.06	-2.94	.005	0.05	0.06	0.86	.387	-0.22	0.06	-3.56	.001
Left middle cingulate gyrus	6.16	0.008	-0.17	0.06	-2.90	.006	0.03	0.06	0.54	.588	-0.20	0.06	-3.21	.004
Right medial frontal cortex	10.55	<.001	-0.14	0.05	-2.85	.007	0.10	0.05	2.02	.043	-0.23	0.05	-4.56	<.001
Left medial frontal cortex	9.53	<.001	-0.11	0.05	-2.21	.028	0.12	0.05	2.44	.022	-0.23	0.05	-4.36	<.001
Right middle frontal gyrus	17.16	<.001	-0.22	0.06	-3.75	<.001	0.14	0.06	2.40	.017	-0.36	0.06	-5.80	<.001
Left middle frontal gyrus	15.16	<.001	-0.22	0.06	-3.66	<.001	0.13	0.06	2.09	.037	-0.35	0.06	-5.43	<.001
Right medial orbital gyrus	4.60	0.025	-0.04	0.03	-1.41	.158	0.05	0.03	1.79	.110	-0.09	0.03	-3.03	.008
Left medial orbital gyrus	3.89	0.039	-0.05	0.03	-1.61	.160	0.04	0.03	1.34	.182	-0.09	0.03	-2.79	.016
Right postcentral gyrus medial segment	4.16	0.032	-0.16	0.06	-2.55	.020	0.01	0.07	0.12	.908	-0.17	0.07	-2.49	.020
Right precentral gyrus medial segment	3.71	0.045	-0.14	0.07	-2.12	.051	0.04	0.07	0.63	.530	-0.18	0.07	-2.57	.031
Right superior frontal gyrus medial segment	16.96	<.001	-0.26	0.06	-4.54	<.001	0.08	0.06	1.30	.195	-0.34	0.06	-5.50	<.001
Left superior frontal gyrus medial segment	16.34	<.001	-0.27	0.06	-4.51	<.001	0.07	0.06	1.17	.241	-0.34	0.06	-5.36	<.001
Right middle temporal gyrus	4.96	0.019	-0.06	0.04	-1.46	.145	0.08	0.04	1.89	.089	-0.14	0.05	-3.14	.005
Right opercular part of the inferior frontal gyrus	13.26	<.001	-0.17	0.06	-2.92	.005	0.15	0.06	2.54	.011	-0.33	0.06	-5.14	<.001

			S1-TD				S2-TD				S1-S2			
	F	***p***	***B***	***SE***	***t***	p_{fdr}	***B***	***SE***	***t***	p_{fdr}	***B***	***SE***	***t***	p_{fdr}
Left opercular part of the inferior frontal gyrus	10.93	<.001	-0.18	0.06	-2.88	.006	0.13	0.06	2.06	.040	-0.31	0.07	-4.65	<.001
Right orbital part of the inferior frontal gyrus	4.14	0.032	-0.06	0.05	-1.16	.245	0.09	0.05	1.86	.096	-0.15	0.05	-2.85	.014
Left orbital part of the inferior frontal gyrus	5.01	0.019	-0.06	0.05	-1.16	.247	0.12	0.05	2.14	.049	-0.18	0.06	-3.11	.006
Right parahippocampal gyrus	4.14	0.032	-0.06	0.03	-1.92	.083	0.03	0.03	1.08	.281	-0.09	0.03	-2.83	.014
Right postcentral gyrus	5.17	0.017	-0.16	0.06	-2.51	.019	0.05	0.06	0.74	.461	-0.21	0.07	-3.03	.007
Left postcentral gyrus	4.61	0.025	-0.15	0.06	-2.51	.018	0.03	0.06	0.45	.653	-0.18	0.06	-2.77	.017
Right posterior orbital gyrus	6.09	0.008	-0.08	0.03	-2.42	.024	0.04	0.03	1.22	.222	-0.12	0.03	-3.41	.002
Right planum polare	8.44	0.001	-0.09	0.05	-1.84	.066	0.13	0.05	2.50	.019	-0.22	0.05	-4.09	<.001
Left planum polare	5.41	0.014	-0.10	0.05	-2.00	.069	0.07	0.05	1.48	.140	-0.17	0.05	-3.27	.003
Right precentral gyrus	7.41	0.003	-0.18	0.06	-3.01	.004	0.05	0.06	0.86	.388	-0.23	0.06	-3.62	.001
Left precentral gyrus	4.82	0.021	-0.16	0.06	-2.57	.016	0.03	0.06	0.46	.644	-0.18	0.06	-2.83	.014
Right superior frontal gyrus	13.99	<.001	-0.22	0.06	-3.85	<.001	0.09	0.06	1.58	.115	-0.30	0.06	-5.12	<.001
Left superior frontal gyrus	11.27	<.001	-0.19	0.06	-3.39	.001	0.09	0.06	1.50	.134	-0.28	0.06	-4.61	<.001
Right supplementary motor cortex	8.97	0.001	-0.20	0.06	-3.24	.002	0.06	0.06	1.06	.288	-0.26	0.06	-4.03	<.001
Left supplementary motor cortex	6.30	0.007	-0.16	0.06	-2.62	.013	0.06	0.06	1.03	.303	-0.22	0.07	-3.42	.002
Right supramarginal gyrus	3.82	0.041	-0.12	0.06	-2.12	.052	0.04	0.06	0.69	.493	-0.16	0.06	-2.62	.027
Left supramarginal gyrus	5.64	0.012	-0.14	0.05	-2.65	.012	0.04	0.05	0.73	.468	-0.18	0.06	-3.15	.005
Right superior parietal lobule	3.86	0.040	-0.13	0.06	-2.29	.034	0.02	0.06	0.44	.662	-0.15	0.06	-2.55	.033
Left superior parietal lobule	4.50	0.025	-0.11	0.06	-1.96	.075	0.07	0.06	1.20	.229	-0.18	0.06	-2.96	.009
Right superior temporal gyrus	4.24	0.031	-0.07	0.05	-1.22	.223	0.10	0.05	1.85	.096	-0.17	0.06	-2.89	.012
Right temporal pole	11.23	<.001	-0.10	0.03	-3.42	.001	0.04	0.03	1.48	.139	-0.15	0.03	-4.59	<.001
Left temporal pole	8.89	0.001	-0.10	0.03	-3.16	.002	0.04	0.03	1.12	.263	-0.13	0.03	-4.04	<.001
Right triangular part of the inferior frontal gyrus	14.28	<.001	-0.14	0.06	-2.60	.009	0.17	0.06	3.05	.004	-0.31	0.06	-5.34	<.001
Left triangular part of the inferior frontal gyrus	7.83	0.002	-0.11	0.06	-1.81	.071	0.14	0.06	2.37	.027	-0.25	0.06	-3.94	<.001

Supplementary Table S11. Group differences in fractional anisotropy of white matter tracts while controlling for race (n=923, df=915).

			S1-TD				S2-TD				S1-S2			
Tract	***F***	p_{fdr}	***B***	***SE***	***t***	p_{fdr}	***B***	***SE***	***t***	p_{fdr}	***B***	***SE***	***t***	p_{fdr}
Left anterior thalamic radiation	7.26	.004	-0.09	0.07	-1.36	.173	0.17	0.07	2.58	.015	-0.26	0.07	-3.76	.001
Right anterior thalamic radiation	4.19	.032	-0.06	0.07	-0.83	.405	0.14	0.07	2.11	.053	-0.20	0.07	-2.81	.015
Right corticospinal tract	4.81	.030	-0.19	0.07	-2.59	.014	0.03	0.07	0.37	.711	-0.21	0.08	-2.79	.014
Left cingulum (hippocampus)	5.28	.024	-0.18	0.07	-2.49	.020	0.06	0.07	0.79	.428	-0.24	0.08	-3.07	.007
Right cingulum (hippocampus)	4.37	.032	-0.15	0.07	-2.02	.065	0.08	0.08	1.06	.287	-0.23	0.08	-2.89	.012
Forceps minor	9.49	.001	-0.21	0.07	-3.14	.003	0.09	0.07	1.31	.190	-0.30	0.07	-4.20	<.001
Left inferior longitudinal fasciculus	3.75	.043	-0.18	0.07	-2.42	.029	0.01	0.08	0.07	.946	-0.18	0.08	-2.34	.029
Right inferior longitudinal fasciculus	7.79	.004	-0.21	0.08	-2.80	.008	0.10	0.08	1.24	.214	-0.31	0.08	-3.82	<.001
Right superior longitudinal fasciculus	4.38	.032	-0.19	0.07	-2.84	.014	-0.04	0.07	-0.53	.597	-0.16	0.07	-2.16	.046
Left uncinate fasciculus	4.16	.032	-0.20	0.07	-2.70	.021	-0.02	0.08	-0.28	.777	-0.18	0.08	-2.26	.036

Supplementary Table S12. Group differences for traditional diagnostic categories (n=1,141, df=1,136).

			S1-S2			
	F	***p***	***B***	***SE***	***t***	p_{fdr}
ADHD	97.63	<.001	0.01	0.09	0.14	.889
Agoraphobia	76.49	<.001	0.31	0.08	3.72	<.001
Anorexia Nervosa	17.33	<.001	0.02	0.05	0.51	.610
Bulimia Nervosa	11.17	<.001	0.01	0.03	0.36	.722
Conduct Disorder	76.14	<.001	0.49	0.08	6.38	<.001
GAD	48.81	<.001	-0.03	0.07	-0.44	.657
Mania	72.47	<.001	0.12	0.07	1.68	.093
MDD	109.27	<.001	0.09	0.10	0.94	.347
OCD	75.31	<.001	0.06	0.08	0.76	.447
ODD	199.53	<.001	0.61	0.11	5.67	<.001
Panic	41.58	<.001	0.09	0.05	1.71	.087
Psychosis	85.17	<.001	0.17	0.09	1.94	.053
PTSD	87.38	<.001	0.37	0.10	3.86	<.001
Separation Anxiety	70.49	<.001	-0.12	0.08	-1.59	.113
Social Anxiety	167.08	<.001	0.24	0.11	2.13	.033

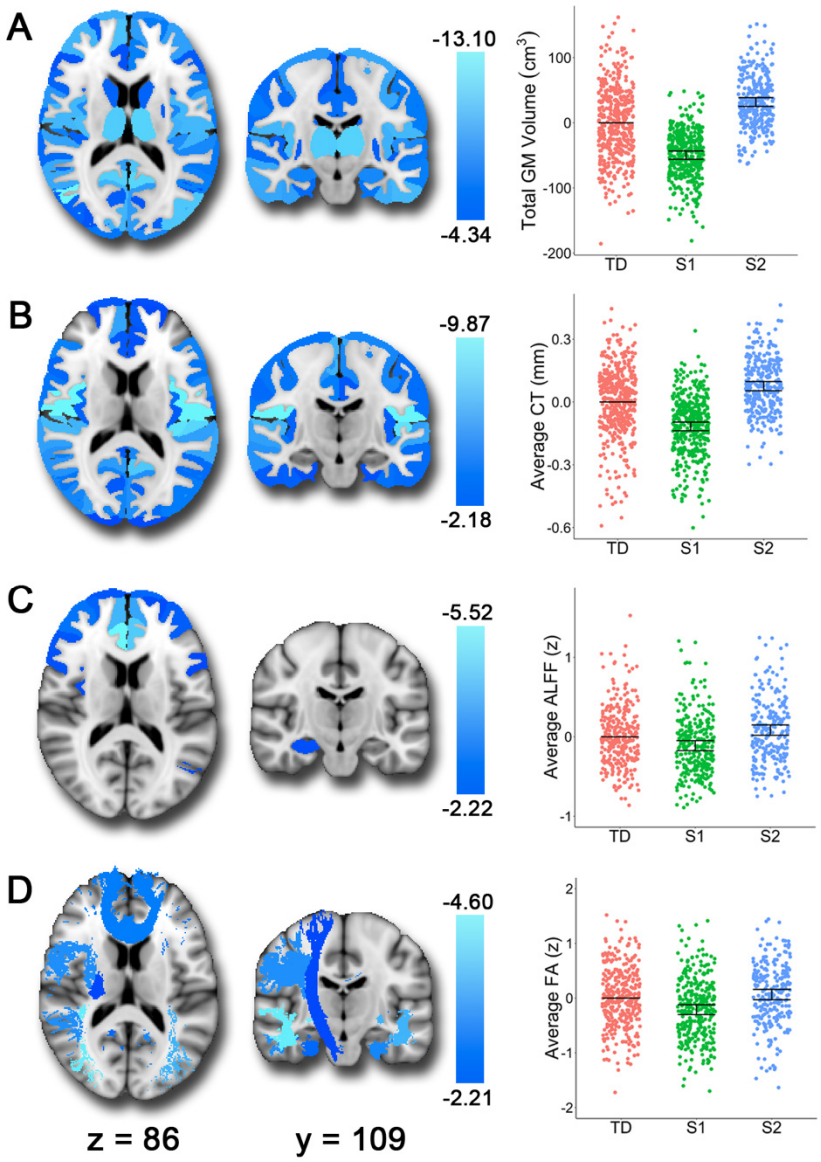

Supplementary Figure S1. Subtype 1 (S1) shows smaller volume, thinner cortex, lower resting-state ALFF, and reduced white matter integrity relative to typically developing youth (TD). The brain images show the t-values for the S1>TD contrast. In the scatterplots, we show the estimates from the fitted GAM model with all three groups for comparison. Each vertical line represents the 95% confidence interval (CI), with the comparison group (TD) represented by its mean line. The subtype is significantly different from TD if its corresponding CI does not contain 0 (the mean of TD). In comparison to TD, S1 showed **A)** smaller volumes, **B)** reduced cortical thickness, **C)** reduced resting-state ALFF (amplitude of low frequency fluctuations) in frontal regions, bilateral amygdala, and right hippocampus, and **D)** reduced fractional anisotropy in white matter tracts including the inferior longitudinal fasciculi, uncinate fasciculus, corticospinal tract, parahippocampal cingulum, superior longitudinal fasciculus, and forceps minor.

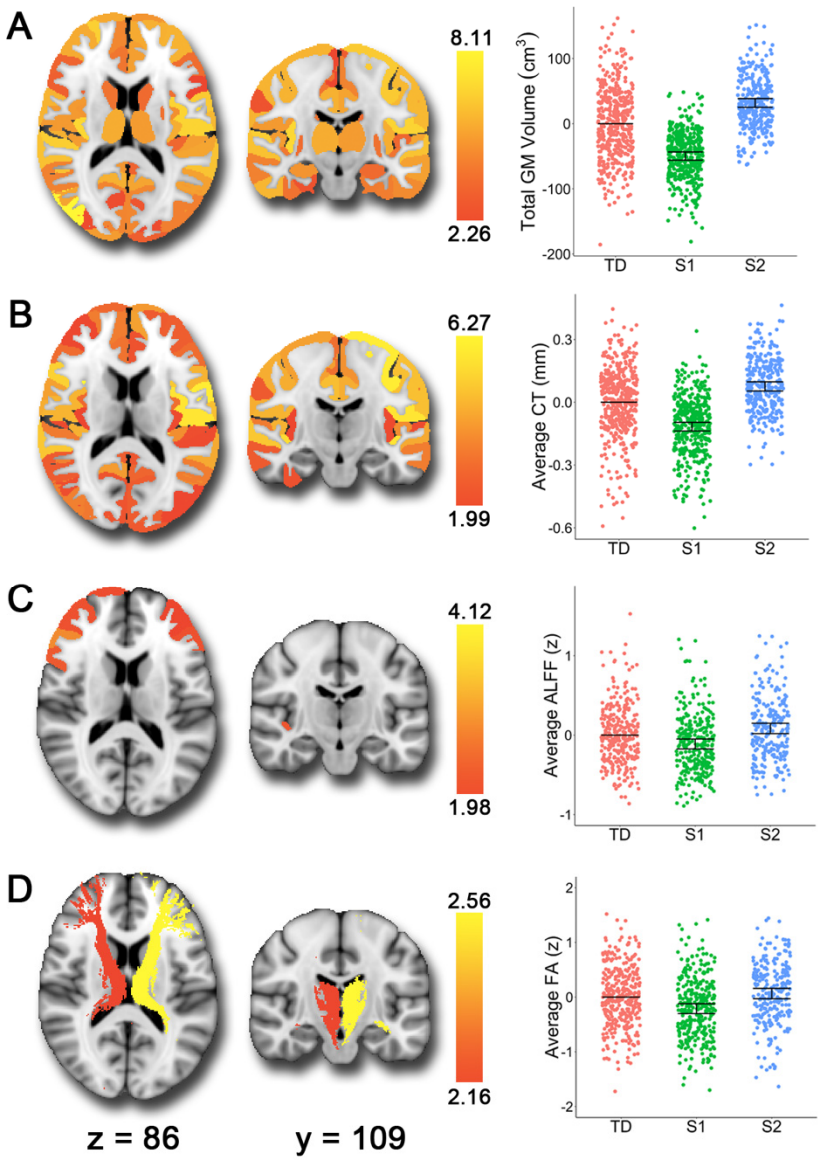

Supplementary Figure S2. Subtype 2 (S2) shows larger volume, thicker cortex, higher resting-state ALFF, and greater white matter integrity relative to typically developing youth (TD). The brain images show the t-values for the S2>TD contrast. In the scatterplots, we show the estimates from the fitted GAM model with all three groups for comparison. Each vertical line represents the 95% confidence interval (CI), with the comparison group (TD) represented by its mean line. The subtype is significantly different from TD if its corresponding CI does not contain 0 (the mean of TD). In comparison to TD, S2 showed **A)** larger volumes, **B)** greater cortical thickness, **C)** higher resting-state ALFF (amplitude of low frequency fluctuations) in frontal regions, and **D)** greater fractional anisotropy in the left and right anterior thalamic radiations.

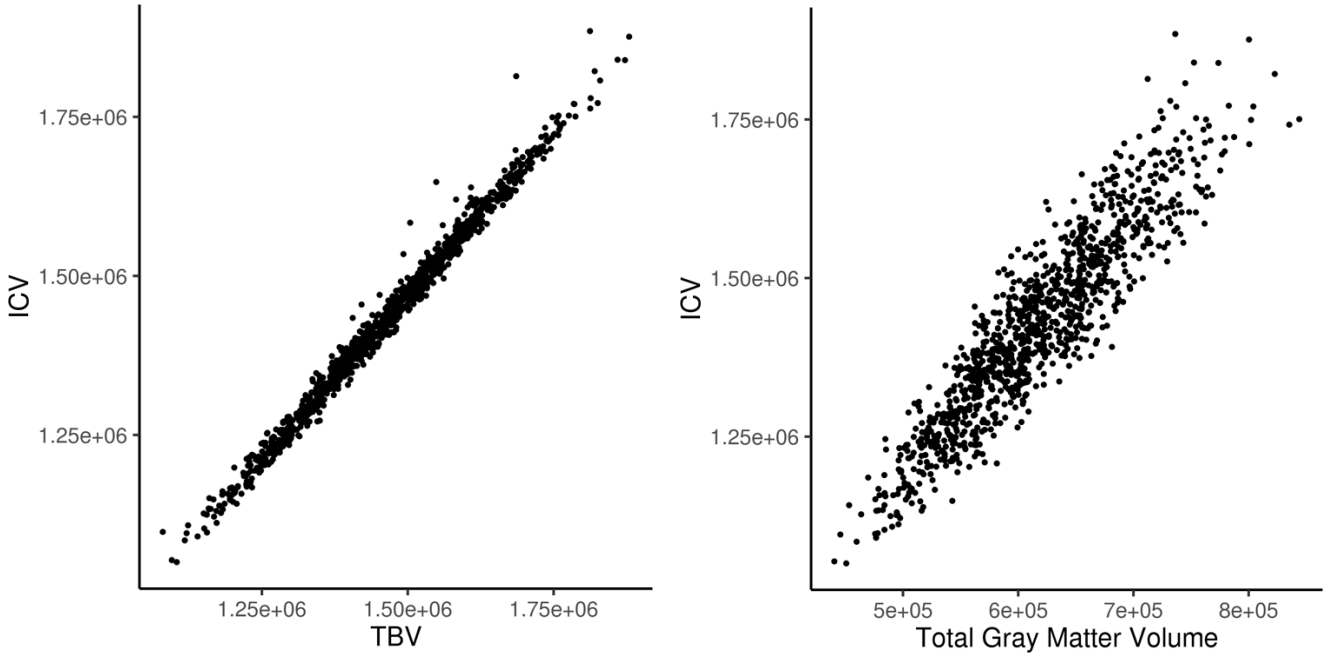

Supplementary Figure S3. Total brain volume (TBV) and total gray matter volume are highly correlated with intracranial volume (ICV). The correlation between ICV and TBV was .99, while the correlation between ICV and total gray matter volume was .92 for the total sample. For correlations by group, see Supplementary Figure S4.

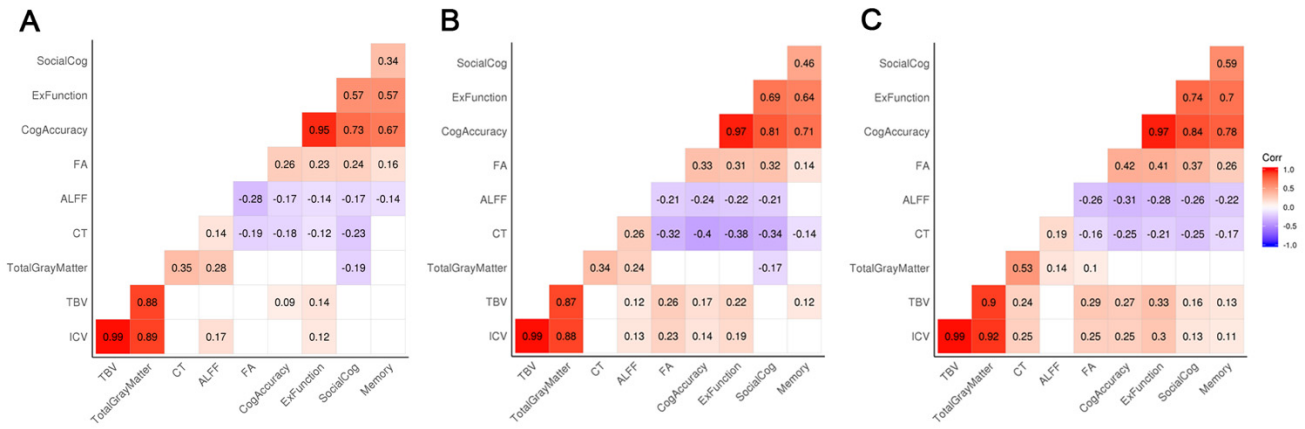

Supplementary Figure S4. Interrelationships between structure, ALFF, FA, and cognition. Correlation coefficients are overlaid on the matrices, with blank squares indicating non-significant correlations (uncorrected). Interrelationships between variables were similar for **A)** Subtype 1, **B)** Subtype 2, and **C)** typically developing youth.

Supplemental References

1. Satterthwaite TD, Connolly JJ, Ruparel K, Calkins ME, Jackson C, Elliott MA, *et al.* (2016): The Philadelphia Neurodevelopmental Cohort: A publicly available resource for the study of normal and abnormal brain development in youth. *Neuroimage*. 124: 1115–1119.
2. Satterthwaite TD, Elliott MA, Ruparel K, Loughead J, Prabhakaran K, Calkins ME, *et al.* (2014): Neuroimaging of the Philadelphia Neurodevelopmental Cohort. *Neuroimage*. 86: 544–553.
3. Gur RE, Kaltman D, Melhem ER, Ruparel K, Prabhakaran K, Riley M, *et al.* (2013): Incidental findings in youths volunteering for brain MRI research. *Am J Neuroradiol*. 34: 2021–2025.
4. Rosen A, Roalf DR, Ruparel K, Blake J, Seelaus K, Villa P, *et al.* (2017): Data-driven Assessment of Structural Image Quality. *Neuroimage*. 169: 407–418.
5. Nassar R, Kaczkurkin AN, Xia CH, Sotiras A, Pehlivanova M, Moore TM, *et al.* (2018): Gestational Age is Dimensionally Associated with Structural Brain Network Abnormalities Across Development. *Cereb Cortex*. 29: 2102–2114.
6. Calkins ME, Merikangas KR, Moore TM, Burstein M, Behr A, Satterthwaite TD, *et al.* (2015): The Philadelphia Neurodevelopmental Cohort: constructing a deep phenotyping collaborative. *J Child Psychol Psychiatry*. 56: 1356–1369.
7. Kaufman J, Birmaher B, Brent D, Rao U, Flynn C, Moreci P, *et al.* (1997): Schedule for Affective Disorders and Schizophrenia for School-Age Children-Present and Lifetime Version (K-SADS-PL): Initial Reliability and Validity Data. *J Am Acad Child Adolesc Psychiatry*. 36: 980–988.
8. American Psychiatric Association (2000): *Diagnostic and Statistical Manual of Mental Health Disorders, Fourth Edition, Text Revision*, 4th Ed., T. Washington, D.C.: American Psychiatric Association.
9. Moore TM, Calkins ME, Satterthwaite TD, Roalf DR, Port AM, Jackson CT, *et al.* (2019): Development, validation, and public release of a computerized adaptive (CAT) screener for overall mental illness burden. under review.
10. Reise SP, Moore TM, Haviland MG (2010): Bifactor models and rotations: Exploring the extent to which multidimensional data yield univocal scale scores. *J Pers Assess*. 92: 544–559.
11. Gibbons RD, Hedeker DR (1992): Full-information item bi-factor analysis. *Psychometrika*. 57: 423–436.
12. Muthén L, Muthén B (2012): *Mplus The Comprehensive Modelling Program for Applied Researchers: Users Guide*. Los Angeles, CA: Muthén and Muthén.
13. Moore TM, Reise SP, Gur RE, Hakonarson H, Gur RC (2015): Psychometric properties of the Penn Computerized Neurocognitive Battery. *Neuropsychology*. 29: 235–46.
14. Wilkinson G, Robertson G (2006): *Wide Range Achievement Test, Fourth Edition*. Lutz, FL: Psychological Assessment Resources, Inc.
15. Avants BB, Tustison NJ, Wu J, Cook PA, Gee JC (2011): An open source multivariate framework for N-tissue segmentation with evaluation on public data. *Neuroinformatics*. 9: 381–400.
16. Das SR, Avants BB, Grossman M, Gee JC (2009): Registration based cortical thickness measurement. *Neuroimage*. 45: 867–879.
17. Tustison NJ, Avants BB, Cook PA, Zheng Y, Egan A, Yushkevich PA, Gee JC (2010): N4ITK: Improved N3 bias correction. *IEEE Trans Med Imaging*. 29: 1310–1320.
18. Avants BB, Tustison NJ, Song G, Cook PA, Klein A, Gee JC (2011): A reproducible evaluation of ANTs similarity metric performance in brain image registration. *Neuroimage*. 54: 2033–2044.
19. Klein A, Ghosh SS, Avants B, Yeo BTT, Fischl B, Ardekani B, *et al.* (2010): Evaluation of volume-based and surface-based brain image registration methods. *Neuroimage*. 51: 214–220.
20. Wang H, Suh JW, Das SR, Pluta JB, Craige C, Yushkevich PA (2013): Multi-atlas segmentation with joint label fusion. *IEEE Trans Pattern Anal Mach Intell*. 35: 611–623.

21. Ciric R, Wolf DH, Power JD, Roalf DR, Baum GL, Ruparel K, *et al.* (2017): Benchmarking of participant-level confound regression strategies for the control of motion artifact in studies of functional connectivity. *Neuroimage*. 154: 174–187.
22. Jenkinson M, Bannister P, Brady M, Smith S (2002): Improved optimization for the robust and accurate linear registration and motion correction of brain images. *Neuroimage*. 17: 825–841.
23. Greve DN, Fischl B (2009): Accurate and robust brain image alignment using boundary-based registration. *Neuroimage*. 48: 63–72.
24. Hallquist MN, Hwang K, Luna B (2013): The nuisance of nuisance regression: Spectral misspecification in a common approach to resting-state fMRI preprocessing reintroduces noise and obscures functional connectivity. *Neuroimage*. 82: 208–225.
25. Yu-feng Z, Yong H, Chao-zhe Z, Qing-jiu C, Man-qiu S, Meng L, *et al.* (2007): Altered baseline brain activity in children with ADHD revealed by resting-state functional MRI. *Brain Dev*. 29: 83–91.
26. Smith SM, Brady JM (1997): SUSAN - A new approach to low level image processing. *Int J Comput Vis*. 23: 45–78.
27. Andersson JLR, Sotiropoulos SN (2016): An integrated approach to correction for off-resonance effects and subject movement in diffusion MR imaging. *Neuroimage*. 125: 1063–1078.
28. Jenkinson M, Beckmann CF, Behrens TEJ, Woolrich MW, Smith SM (2012): FSL. *Neuroimage*. 62: 782–790.
29. Zhang H, Yushkevich PA, Alexander DC, Gee JC (2006): Deformable registration of diffusion tensor MR images with explicit orientation optimization. *Med Image Anal*. 10: 764–785.
30. Zhang B, Xu Y, Zhu B, Kantarci K (2014): The role of diffusion tensor imaging in detecting microstructural changes in prodromal Alzheimer's disease. *CNS Neurosci Ther*. 20: 3–9.
31. Roalf DR, Quarmley M, Elliott MA, Satterthwaite TD, Vandekar SN, Ruparel K, *et al.* (2016): The impact of quality assurance assessment on diffusion tensor imaging outcomes in a large-scale population-based cohort. *Neuroimage*. 125: 903–919.
32. Rosen AFG, Roalf DR, Ruparel K, Blake J, Seelaus K, Villa LP, *et al.* (2018): Quantitative assessment of structural image quality. *Neuroimage*. 169: 407–418.
33. Satterthwaite TD, Elliott MA, Gerraty RT, Ruparel K, Loughead J, Calkins ME, *et al.* (2013): An improved framework for confound regression and filtering for control of motion artifact in the preprocessing of resting-state functional connectivity data. *Neuroimage*. 64: 240–256.
34. Satterthwaite TD, Shinohara RT, Wolf DH, Hopson RD, Elliott MA, Vandekar SN, *et al.* (2014): Impact of puberty on the evolution of cerebral perfusion during adolescence. *Proc Natl Acad Sci*. 111: 8643–8648.
35. Giedd JN, Blumenthal J, Jeffries NO, Castellanos FX, Liu H, Zijdenbos A, *et al.* (1999): Brain development during childhood and adolescence: a longitudinal MRI study. *Nat Neurosci*. 2: 861–863.
36. Lenroot RK, Gogtay N, Greenstein DK, Wells EM, Wallace GL, Clasen LS, *et al.* (2007): Sexual dimorphism of brain developmental trajectories during childhood and adolescence. *Neuroimage*. 36: 1065–1073.
37. Wood SN (2004): Stable and efficient multiple smoothing parameter estimation for generalized additive models. *J Am Stat Assoc*. 99: 673–686.
38. Wood SN (2001): mgcv: GAMs and generalized ridge regression for R. *R News*. 1: 20–25.
39. Kaczkurkin AN, Raznahan A, Satterthwaite TD (2019): Sex differences in the developing brain: insights from multimodal neuroimaging. *Neuropsychopharmacology*. 44: 71–85.
40. Nichols TE, Holmes AP (2001): Nonparametric Permutation Tests for Functional Neuroimaging: A Primer with Examples. *Hum Brain Mapp*. 15: 1–25.